ACS Sustainable Chemistry & Engineering

pubs.acs.org/journal/ascecg

Research Article

Spatially Resolved Reaction Profiles of CO_2 Hydrogenation to Methanol Using In-Based Catalysts in a Compact Profile Reactor

Philipp Kampe,[⊥] Nick Herrmann,[⊥] Charlotte Ruhmlieb, Maik Finsel, Oliver Korup, Raimund Horn, and Jakob Albert*

Cite This: *ACS Sustainable Chem. Eng.* 2024, 12, 9541−9549

Read Online

ACCESS | Metrics & More | Article Recommendations | Supporting Information

ABSTRACT: The compact profile reactor (CPR) design allows for the simultaneous acquisition of species, temperature, and spatially resolved reaction profiles during high-pressure CO_2 hydrogenation to methanol. Indium-based catalysts for CO_2 hydrogenation have attracted significant scientific interest since they are more selective, efficient, and resistant to deactivation compared to the state-of-the-art copper-based catalyst. In this study, the reaction profile of In_2O_3/ZrO_2 catalysts is compared to that of the state-of-the-art $Cu/ZnO/Al_2O_3$ (CZA) catalyst in a high-pressure CPR. It is demonstrated that the addition of nickel as a promoter significantly enhanced the catalytic activity of pure In_2O_3/ZrO_2. The characterization by H_2 TPR and CO_2 TPD revealed an increased capacity for both hydrogen and CO_2. A detailed comparison and optimization of reaction conditions using $Ni-In_2O_3/ZrO_2$ as a catalyst are presented. In an optimized experiment, $Ni-In_2O_3/ZrO_2$ produces 4.90 g_{MeOH} g_{In+Ni}^{-1} h^{-1} at 275 °C, 50 bar, and 63,000 $h^{-1}$with a methanol selectivity of 73%. Furthermore, no catalyst deactivation caused by metal leaching or sintering could be observed over 90 h time on stream.

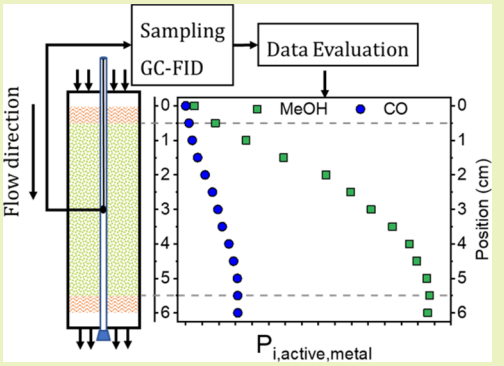

KEYWORDS: *methanol synthesis, compact profile reactor, CO_2 hydrogenation, indium oxide catalyst, Ni doping, hydrogen spillover*

INTRODUCTION

The CO_2 emissions rise since the industrial revolution and have a significant effect as a greenhouse gas for global warming.[1] A promising approach for greenhouse gas reduction is the valorization of CO_2 from industrial off-gases with renewable hydrogen into valuable and sustainable products such as methanol.[2] Different reactor designs have already been employed for this task but were not thoroughly examined yet.

Industrial fixed-bed methanol reactors can be categorized into two types based on the approach used for heat removal within the catalyst bed: (A) adiabatic and (B) isothermal reactors.[3] A typical adiabatic reactor consists of multiple catalyst beds (up to five) arranged in series within a single pressurized shell and with direct cooling (quench) or interstage heat exchange. For example, the *ICI* low-pressure quench converter operates at 50−100 bar and 270 °C by using the $Cu/ZnO/Al_2O_3$ (CZA) catalyst in a single bed. The quench gas is injected and distributed into the bed by lozenges. These traverse horizontally across the converter from one side to the other. A central pipe is used to feed the cold gas. The addition of cold, fresh, and recycled syngas helps to alleviate the reaction temperature. Caused by the variable void fraction along the catalyst bed, each catalyst pellet does not receive the same gas flow, resulting in irregular flux distribution. Thus, both hot and cold zones can be located in the bed.[4] Thermal sintering of the CZA occurs at temperatures above 300 °C and leads to deactivation.[5] Lower temperatures, on the other hand, decelerate the reaction rate.

The *Lurgi* (now Air Liquide) converter, an isothermal reactor, is widely used in the industry for methanol synthesis. Typical operating conditions range from 50 to 100 bar and from 230 to 365 °C.[4] An isothermal reactor integrates plates or tubes in the catalytic bed for heat removal and a more uniform distribution of the temperature. A shell-and-tube design supplies boiling water to the shell side, removing the reaction heat released by the catalyst on the tube side. Consequently, this approach ensures enhanced productivity, prolonged catalyst life, reduced byproduct formation, efficient recovery of reaction heat, and lower operating costs. The design with helically arranged tubes prevents catalytic stress caused by axial temperature variations, which is a classic problem in straight fixed-bed reactors.[3,4]

Although the temperature can be controlled in both reactors, they lack a fundamental understanding of gas-phase composition throughout the catalyst bed since there are only

Received: April 19, 2024
Revised: May 28, 2024
Accepted: May 29, 2024
Published: June 7, 2024

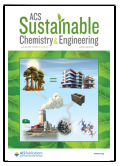

integral measurements for the reactors possible due to the reactor design. The main reactions in methanol synthesis are provided below.

$$CO + 2H_2 \rightleftharpoons CH_3OH \quad \Delta H_R^{\varnothing} = -91\ kJ\ mol^{-1} \tag{1}$$

$$CO_2 + 3H_2 \rightleftharpoons CH_3OH + H_2O \quad \Delta H_R^{\varnothing} = -49\ kJ\ mol^{-1} \tag{2}$$

$$CO_2 + H_2 \rightleftharpoons CO + H_2O \quad \Delta H_R^{\varnothing} = +41\ kJ\ mol^{-1} \tag{3}$$

The common industrial approach for methanol synthesis is using syngas (1) in combination with the state-of-the-art $Cu/ZnO/Al_2O_3$ catalyst.[6] The major compounds of syngas are CO and H_2, while small amounts of CO_2 are added for an increase in catalyst activity.[7] Compared to the CO hydrogenation, the CO_2 hydrogenation generates less reaction heat (2) and the endothermic rWGS (3) attenuates heat release in the process. The formation of water on the surface of the catalyst leads to deactivation by segregating Cu/ZnO and interrupting the strong metal−support interaction effect that is required for the catalyst activity.[8] In the presence of CO_2, water and CO are formed via the competitive reverse water−gas shift reaction (rWGS, 3), which lowers the methanol selectivity. To enhance the stability of CZA and to shift the thermodynamic equilibrium toward methanol (according to Le Chatelier's principle), water can be removed in situ with novel membrane reactors (laboratory level).[9] A slurry reactor concept using a carrier thermoliquid with the advantages of a simple construction, facile reactor control, and efficient heat storage has been already employed in more recent studies.[10−12] Reducing particle sizes in slurry reactors allows for their use without the necessity to account for pressure drop along a catalyst bed. Additionally, this results in less attrition of the catalyst particles. Gaikwand et al. split the commercial CZA catalyst into three catalyst beds separated by empty sections.[13] This study showed that methanol is produced through high-pressure direct CO_2 hydrogenation at low temperatures, while above 260 °C, methanol formation is facilitated by CO, which is generated through the rWGS reaction.

Indium-based catalysts have recently been studied extensively as alternative methanol synthesis catalysts by CO_2 hydrogenation.[14−18] The ZrO_2 supported In_2O_3 catalyst also showed high stability, selectivity, and activity for CO_2 hydrogenation to methanol.[10,16,19−29] In previous studies by Wesner and Kampe et al., the effects of the catalyst support, synthesis method, and metal promoter were identified to be key factors to increase the catalytic performance in the CO_2 hydrogenation to methanol.[17]

The objective of this paper is to provide first insights into spatially resolved measurements on indium-based methanol synthesis catalysts using a novel compact profile reactor (CPR) under high-pressure operating conditions. The CPR offers insights into reactant composition and temperature profiles in a scalable reactor tube and is already established at mild reaction conditions for various heterogeneously catalyzed reactions.[30−33] In this work, we adapt a modified CPR to high-pressure methanol synthesis conditions and compare the reaction profiles of various indium-based catalysts to those of the commercial copper-based catalyst. In detail, the state-of-the-art $Cu/ZnO/Al_2O_3$ catalyst in relation to an In_2O_3/ZrO_2 catalyst will be spatially examined and discussed. Moreover, metal-promoted indium-based catalysts will be further investigated with a specific focus on the influence of certain reaction parameters like pressure, GHSV, and temperature using the most promising catalyst.

EXPERIMENTAL DETAILS

Materials. The following reagents were used as precursors for catalyst synthesis: zirconium dioxide pellets (ZrO_2, Saint Gobain), indium nitrate ($In(NO_3)_3$, 99.999% Thermo Fisher Scientific), cerium nitrate hexahydrate ($Ce(NO_3)_3{\cdot}6H_2O$, 99.5% Thermo Fisher Scientific), copper nitrate trihydrate ($Cu(NO_3)_2{\cdot}3H_2O$, 99% Thermo Fisher Scientific), and nickel nitrate hexahydrate ($Ni(NO_3)_2{\cdot}6H_2O$ 99%, Sublab). A commercial copper-based catalyst ($CuO/ZnO/Al_2O_3$) was purchased from Alfa Aesar (product no. 45776). A gas mixture of hydrogen and carbon dioxide (25% CO_2, 4.5 grade and 75% H_2, 5.0 grade) from Westfalen was used for the catalytic experiments in the CPR reactor. Nitrogen (N_2, 5.0 grade, Linde) was used as a purging gas, and hydrogen (H_2, 5.0 grade, Linde) was used for the catalyst preforming. All chemicals were used as received without further purification.

Catalyst Synthesis. An In_2O_3/ZrO_2 catalyst with 10 wt % of indium loading was prepared by wet impregnation according to previously published methods.[16] Zirconium dioxide pellets were first crushed and sieved to a particle size of 80−250 μm. $In(NO_3)_3$ (6.84 g) was dissolved in a solution of ethanol and deionized water (3:1, 850 mL), and ZrO_2 (18 g, 80−250 μm) was added. The suspension was stirred for 5 h (21 °C, 800 mbar), and the solvent was removed at elevated temperature and reduced pressure (70 °C, 200 mbar) afterwards. The residue was dried for 12 h (65 °C) and calcined for 3 h (300 °C, ramp of 5 °C min^{-1}) in a muffle furnace.

The synthesis of the metal-promoted M-In_2O_3/ZrO_2 catalysts with 1 wt % of promoter was done by wet impregnation. Metal nitrate was dissolved in deionized water (250 mL), and In_2O_3/ZrO_2 (15 g) was added. The suspension was stirred for 5 h (21 °C, 800 mbar), and the solvent was removed at elevated temperature and reduced pressure (70 °C, 200 mbar) afterwards. The residue was dried for 12 h (65 °C) and calcined for 3 h (300 °C, ramp of 5 °C min^{-1}).

Catalyst Characterization. Inductively coupled plasma optical emission spectroscopy (ICP-OES) was used for determining the elementary composition of the catalysts. Hereby, 100 mg of a catalyst sample was digested in 5 mL of conc. H_2SO_4 and 1 mL of fuming HNO_3. It was then atomized in an argon plasma, and the composition was quantified using optical emission spectroscopy. The characterization was carried out on an *ASCOR-spectrometer* (Fa. Spectro) by the central element analysis service (Department of Chemistry, University of Hamburg).

Nitrogen physisorption was carried out with an *Autosorb iQ-MP/XR* analyzer (Fa. Quantachrome Instruments) at 77 K. First, the sample was degassed at 473 K at reduced pressure for 10 h prior to analysis. Using the Brunauer−Emmett−Teller (BET) model, the specific surface area of the sample was determined, and the pore volume was calculated by using the Barrett−Joyner−Halenda (BJH) model.

Temperature-programmed desorption of CO_2 (CO_2 TPD) and temperature-programmed reduction by H_2 (H_2 TPR) were measured using a *ChemBET Pulsar* (Fa. Quantachrome Instruments). Prior to CO_2 TPD, samples (0.3 g) were exposed to a He gas flow (80 mL/min) and heated up to 200 °C (10 K/min) for 1 h to remove surface H_2O. The loading of the surface with CO_2 was also carried out at 200 °C, followed by cooling to 50 °C. The sample was thereafter heated under a He gas flow (80 mL/min, 10 °C/min) to 700 °C, and the desorbed CO_2 was measured via a thermal conductivity detector (TCD). Prior to H_2 TPR, samples (0.3 g) were exposed to a N_2 gas flow (80 mL/min) and heated up to 180 °C (10°/min) for 1 h to remove surface H_2O, followed by cooling to 100 °C. The sample was heated again under a H_2/N_2 (5/95 v/v) gas flow (80 mL/min, 10 °C/min) to 850 °C. The used H_2 was measured by a thermal conductivity detector (TCD).

Powder X-ray diffraction (p-XRD) was carried out using a *Panalytical MDP X'Pert Pro* diffractometer using Cu Kα (λ = 0.1541 nm) radiation. The measuring range of the diffraction angle

https://doi.org/10.1021/acssuschemeng.4c03279
ACS Sustainable Chem. Eng. 2024, 12, 9541−9549

was 10−80° and sampled using a rate of 0.013° with a counting time of 0.3 s. In_2O_3 particle sizes were calculated using a modified Scherrer equation[34] based on the characteristic diffraction reflections as described in the Supporting Information, eq S5. The XRD patterns for indium-based catalysts can be found in Figure S2.

Scanning transmission electron microscopy (SEM) was used to obtain images of the sample surface. A *Zeiss LEO Gemini 1550* equipped with a field emission gun and a beam energy of 20 kV was used. Energy-dispersive X-ray spectroscopy (EDX) elemental maps were obtained by using an *Ultim Max* 100 silicon drift detector from Oxford Instruments. The SEM-EDX elemental mappings for all synthesized indium-based catalysts can be found in Figure S3.

Implementation of the Compact Profile Reactor (CPR) for High-Pressure Methanol Synthesis. CO_2 hydrogenation to methanol was carried out using a CPR (see Figure 1, Reacnostics GmbH, Hamburg, Germany). The stainless-steel reactor tube (length: 182 mm; inner diameter: 4 mm; outer diameter: 6 mm) was filled with a 50 mm-long catalyst bed. The catalyst bed was fixated in between two 5 mm quartz wool plugs. Through the catalyst bed, a stainless-steel capillary with four orifices in the wall (diameter: 75 μm) is placed at a defined position inside the reactor tube. Inside the capillary at the location of the four bores, the temperature of the catalyst bed is measured by a thermocouple. The reactor is installed on a guide rail, enabling movement along the capillary in the axial direction. This allows spatially resolved sampling of the gas phase through the orifices and measurement of the temperature in the catalyst bed using a thermocouple in the capillary (see Figure 1).

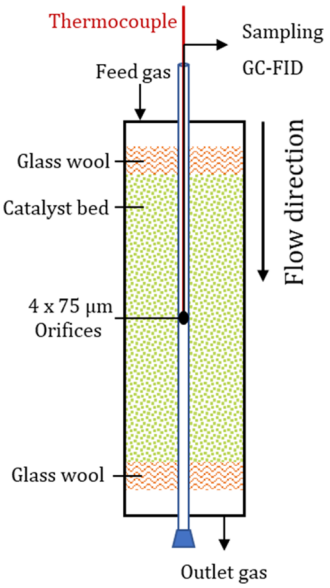

Figure 1. Graphical scheme of the compact profile reactor (CPR).

The capillary for sampling was connected to an online gas chromatograph (Bruker 450-GC), furnished with one thermal conductivity detector (TCD), two flame ionization detectors (FIDs), one methanizer, and four gas chromatography columns (Restek Q-Bond, Restek U-Bond, Bruker Swax, Bruker Molsieve 5 Å) to analyze the gas composition. For more details about the experimental setup, see Figure S1.

Calculations. The active metal productivities of methanol and CO $P_{i,\text{active metal}}$ are defined as the mass flow of the component $\dot{m}_{i,\text{out}}$ related to the active mass of the metal catalyst, which is the mass of the catalyst m_{cat} multiplied with the sum of the active metal $\sum\omega_{\text{active metal}}$

$$P_{i,\text{active metal}} = \frac{\dot{m}_{i,\text{out}}}{m_{\text{cat}} \times (\Sigma\omega_{\text{active metal}})} \tag{4}$$

The selectivity S_i for product i is calculated by determining the ratio of the desired product molar flow to the molar flow of consumed CO_2

$$S_i = \frac{\dot{n}_{i,\text{out}} - \dot{n}_{i,\text{in}}}{\dot{n}_{\text{CO}_2,\text{in}} - \dot{n}_{\text{CO}_2,\text{out}}} \times 100\% \tag{5}$$

The gas hourly space velocity (GHSV) was employed to establish a relationship between the standard volume flow ($\dot{V}_N$) and the catalyst volume (V_{cat})

$$\text{GHSV} = \frac{\dot{V}_N}{V_{\text{cat}}} \tag{6}$$

More details for the calculations are provided in the Supporting Information, eqs S1−S4.

RESULTS AND DISCUSSION

At first, the CPR was set up to run at the desired reaction temperature and pressure of up to 275 °C and 75 bar, respectively. A control experiment with glass beads was performed to investigate the volume-induced pressure drop and to exclude any blind activity. No catalytic activity was

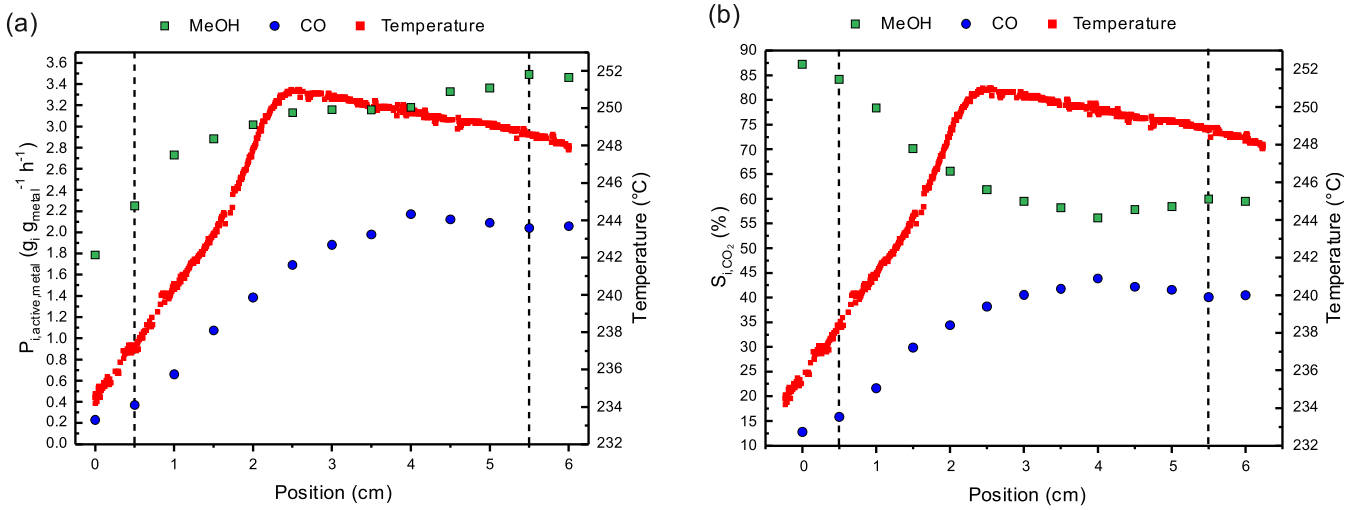

Figure 2. Spatially resolved temperature and product profile of CZA at T = 250 °C, p = 50 bar, GHSV = 63,000 h^{-1}, and a feed gas composition of CO_2/H_2 = 1/3. The measurements were taken between 5 and 35 h TOS. (a) Active metal productivity and (b) selectivity to MeOH (green) and CO (blue) and temperature profile (red).

https://doi.org/10.1021/acssuschemeng.4c03279
ACS Sustainable Chem. Eng. 2024, 12, 9541−9549

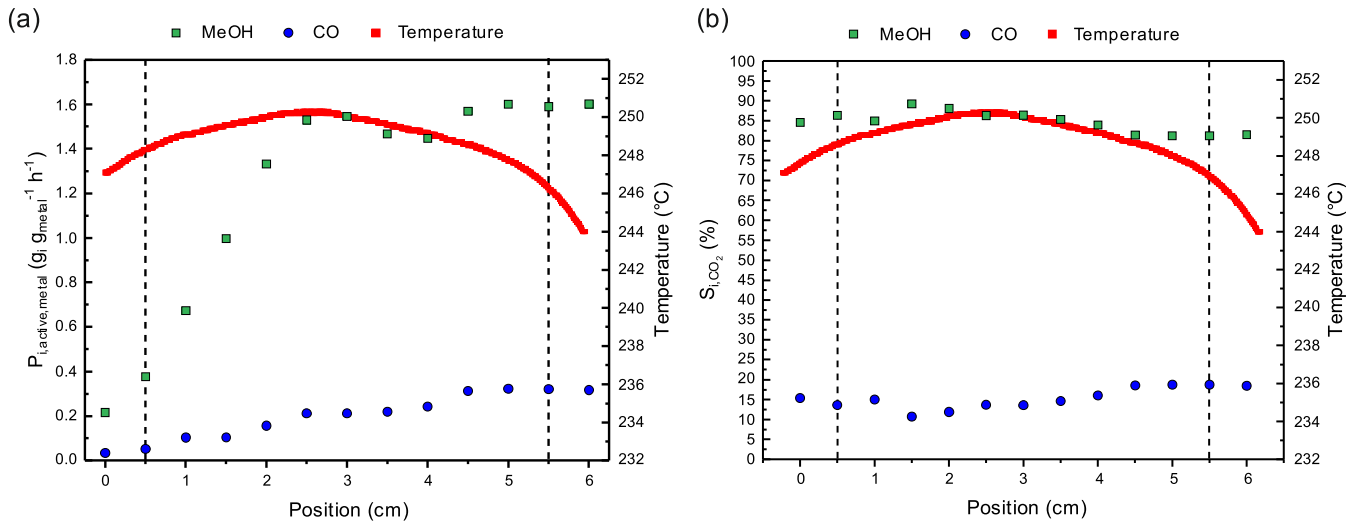

Figure 3. Spatially resolved temperature and product profile of In_2O_3/ZrO_2 at T = 250 °C, p = 50 bar, GHSV = 63,000 h^{-1}, and a feed gas composition of CO_2/H_2 = 1/3. The measurements were taken between 5 and 35 h TOS. (a) Active metal productivity and (b) selectivity of MeOH (green) and CO (blue) and temperature profile (red).

observed. At the maximum gas flow rate of 900 mL_N min^{-1} (GHSV = 95,000 h^{-1}), CO_2/H_2 = 1/3 at 75 bar, a pressure drop below 0.2 bar was determined and can be neglected. For the In_2O_3-ZrO_2 catalyst, a range of 60−250 μm particle size showed the absence of internal mass transfer limitations according to the Weisz−Prater criterion of 0.015.[35] Therefore, a particle size range between 80 and 250 μm was applied for the CPR.

Applying the CPR Reactor for the Commercial Cu/ZnO/Al_2O_3 Catalyst. The catalyst of choice for industrial-scale fossil fuel-based methanol synthesis is the Cu/ZnO/Al_2O_3 catalyst (CZA). An alternative renewable approach is CO_2 hydrogenation using hydrogen from water electrolysis and CO_2 from industrial exhaust gases.[29] While the CZA catalyst is highly active and stable for CO hydrogenation, it deactivates under CO_2 hydrogenation reactions due to the formation of water.[5] The characteristic properties of methanol catalysts strongly depend on both the applied CO amount and reaction conditions. The reaction profile of the CZA for methanol and the byproduct CO due to rWGS is shown in Figure 2 at 50 bar, 250 °C, GHSV = 63,000 h^{-1}, and a feed gas composition of CO_2/H_2 = 1/3. The measurements were taken after reaching steady-state conditions at 5 h time on stream (TOS) for each measurement point. The thermocouple inside the capillary measures the temperature of the gas flow at a certain position. An increase in temperature from the beginning of the catalyst bed was observed up to a maximum of 251 °C at 2.5 cm packing height. This can be attributed to the direct methanol formation by CO_2, which is exothermic. The competing endothermic rWGS reaction increases in the same reaction volume, buffering the temperature, leading to a slight decrease from the maximum. At about 4 cm of the catalyst bed, we observed the highest formation rate of CO (2.17 $g_{CO}\cdot g_{Cu}^{-1}\cdot h^{-1}$) and no significant change until the end of the catalyst bed (see Figure 2a). Presumably, the catalyst bed reached the highest temperature at this point, and from this point on, there is no significant change in the formation of MeOH or CO with a longer packing height. The selectivity of methanol stabilizes at around 58% (see Figure 2b). Over the entire catalytic bed, the active methanol productivity increases to 3.46 $g_{MeOH}\cdot g_{Cu}^{-1}\cdot h^{-1}$ at 6 cm.

For the CZA catalyst, Nielsen et al. concluded that at high conversions, the rate of methanol formation is optimal with a higher CO content. This can be traced back to the ability of CO to remove inhibiting surface-bound water via the WGS reaction.[36] Because of this effect, the methanol formation can be increased a little further at the end of the catalyst bed.

After 55 h time on steam, the active productivity at the reactor outlet decreased to 3.01 $g_{MeOH}\cdot g_{Cu}^{-1}\cdot h^{-1}$. The deactivation is a result of the accelerated crystallization of copper and zinc oxide induced by the byproduct water.[37,38]

Applying the CPR Reactor for the In_2O_3/ZrO_2 Catalyst. A well-discussed and promising alternative catalyst for the direct CO_2 hydrogenation to methanol is the In_2O_3/ZrO_2 catalyst. While the CZA catalyst is sensitive to temperatures above 300 °C and in situ water formation (44% loss in activity over 100 h time on stream), the In_2O_3/ZrO_2 shows no loss in stability during 1000 h time on stream.[16] For the first time, the spatial resolution of the product formation and temperature profile in the catalyst bed was performed using the CPR at 50 bar, 250 °C, GHSV = 63,000 h^{-1}, and a feed gas composition of CO_2/H_2 = 1/3. The measurements were taken under steady-state conditions after 5 h of TOS and 5 h for each measurement point (Figure 3). In comparison to the CZA, less methanol (1.60 $g_{MeOH}\cdot g_{In}^{-1}\cdot h^{-1}$ between 5.0 and 5.5 cm) and CO (0.32 $g_{MeOH}\cdot g_{In}^{-1}\cdot h^{-1}$) was produced (see Figure 3a). Therefore, less reaction heat is released and a lower temperature profile (between 244 and 250 °C) was observed. The lower catalytic activity of In_2O_3/ZrO_2 compared to that of CZA can be explained by the smaller surface area of 74 $m^2\cdot g^{-1}$ for In_2O_3/ZrO_2 compared to the 99 $m^2\cdot g^{-1}$ for CZA (Table S2). The high methanol selectivity varies slightly throughout the length of the catalyst bed between 81 and 89% (Figure 3b).

Applying the CPR Reactor for the Metal-Promoted In_2O_3/ZrO_2 Catalysts. Building on the work of Frei et al. and Kampe et al.,[11,17,20] it was shown that nickel-promoted In_2O_3/ZrO_2 could enhance the catalytic performance compared to pure In_2O_3/ZrO_2. To determine the spatially resolved difference in catalytic performance, we tested the Ni−In_2O_3/ZrO_2 catalyst in the CPR at the same reaction conditions (p = 50 bar, T = 250 °C, see Figure 4).

https://doi.org/10.1021/acssuschemeng.4c03279
ACS Sustainable Chem. Eng. 2024, 12, 9541−9549

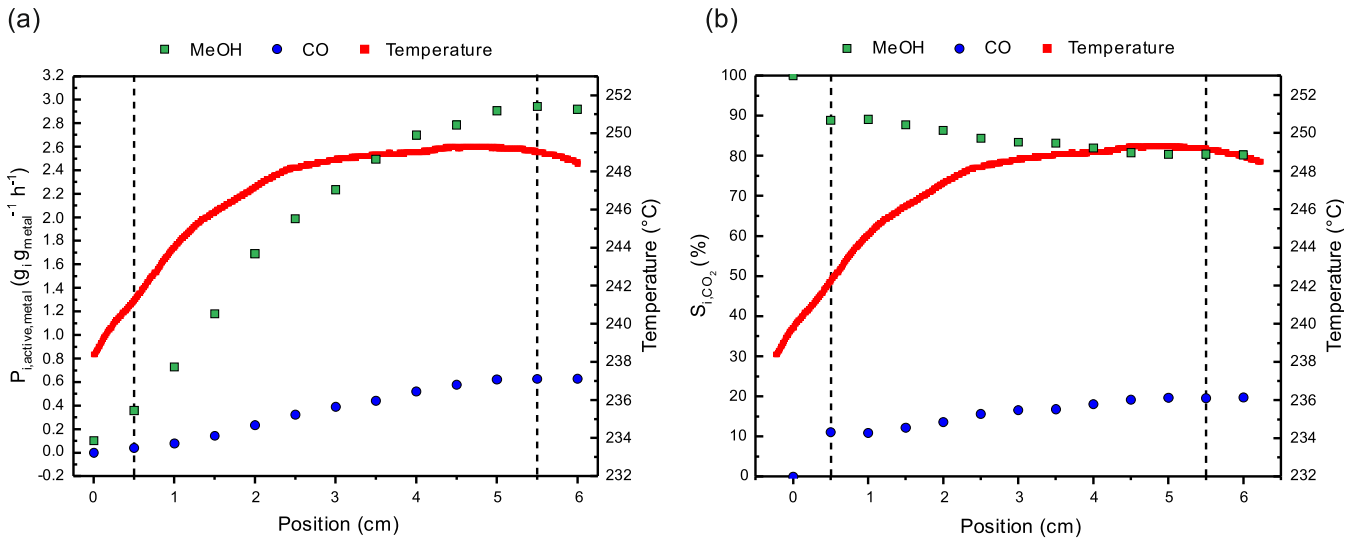

Figure 4. Spatially resolved temperature and product profile of Ni−In_2O_3/ZrO_2 at T = 250 °C, p = 50 bar, GHSV = 63,000 h^{-1}, and a feed gas composition of CO_2/H_2 = 1/3. The measurements were taken between 5 and 35 h TOS. (a) Active metal productivity and (b) selectivity of MeOH (green) and CO (blue) and temperature profile (red).

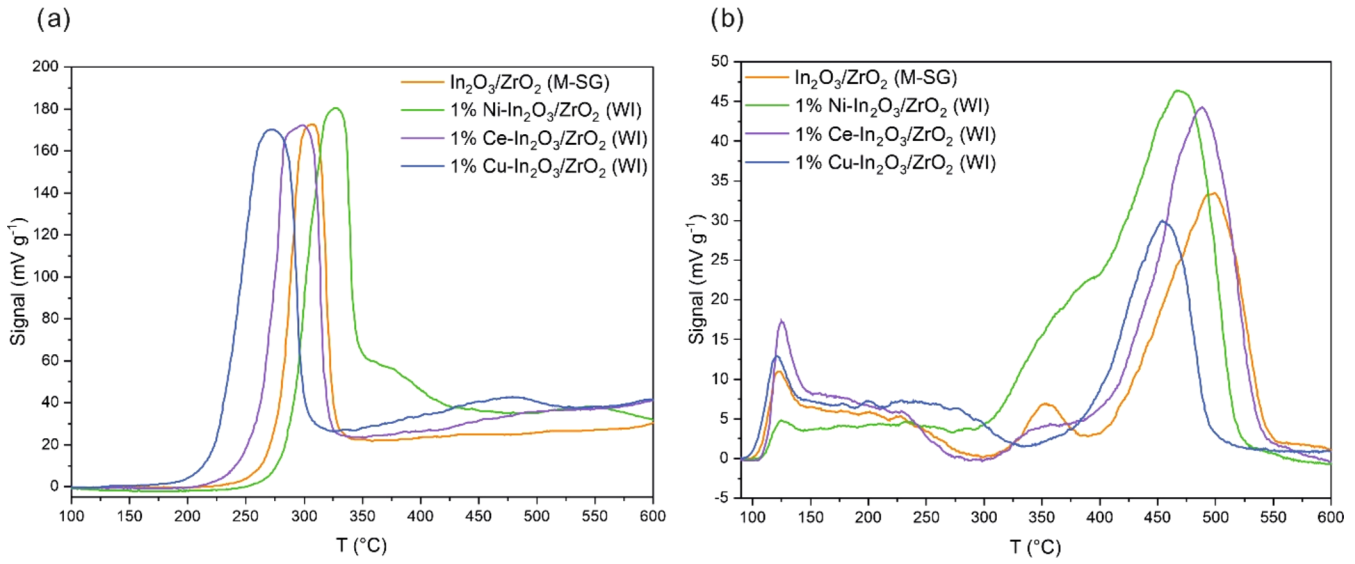

Figure 5. Reducibility and CO_2 adsorption capacity of the In_2O_3/ZrO_2 catalyst compared to the metal-promoted In_2O_3/ZrO_2 catalysts. H_2 TPR (a) and CO_2 TPD (b).

The addition of 0.76 wt % Ni to In_2O_3/ZrO_2 via wetness impregnation (Table S2) shows a tremendous increase in methanol productivity (2.94 $g_{MeOH}{\cdot}g_{In+Ni}^{-1}{\cdot}h^{-1}$ at 5.5 cm) compared to In_2O_3/ZrO_2 (1.59 $g_{MeOH}{\cdot}g_{In}^{-1}{\cdot}h^{-1}$ at 5.5 cm). This can be explained by a higher uptake of hydrogen and CO_2 compared to the other metal-promoted In-based catalysts (Figure 5). Notably, the reduction at temperatures above 350 °C exhibits a distinctive pattern for the nickel-promoted catalysts. The uptake of hydrogen can in part be attributed to the generation of oxygen vacancies, which in turn facilitate CO_2 adsorption and force methanol formation at the In_2O_3/ZrO_2 interface.[39] The vacancies are part of the active sites for CO_2 hydrogenation[40] through the substantially facilitated In_2O_3 reduction as reported by Frei et al.[20] The phenomenon of hydrogen spillover underscores the unique behavior of nickel in the reduction process,[41] contributing to its highest total hydrogen uptake per gram of catalyst. In the context of CO_2 temperature-programmed desorption (CO_2 TPD), the desorption of weakly adsorbed CO_2 occurs at 120 °C across all examined catalysts. Chemically bound CO_2 is subsequently desorbed, providing insights into potential binding sites and their strength. Remarkably, the nickel-promoted catalyst exhibits the highest capacity to adsorb CO_2 compared to that of the other catalysts. Coupled with weaker binding sites, this manifests as a broad shoulder in the temperature range of 300−400 °C and distinguishes the nickel-promoted catalyst from the others. The highest signal area for stronger binding sites could also be attributed to the nickel-promoted catalyst as well (around 475 °C).[20]

An increase of catalyst surface area (80.66 $m^2{\cdot}g^{-1}$) by Ni doping was observed as well, leading to a better accessibility of the reactants. No methanation was observed, which is well in line with the literature.[11,17,20] After 90 h time on stream, the active productivity at the reactor outlet increased slightly from 2.96 $g_{MeOH}{\cdot}g_{In+Ni}^{-1}{\cdot}h^{-1}$ to 3.07 $g_{MeOH}{\cdot}g_{In+Ni}^{-1}{\cdot}h^{-1}$ with no apparent deactivation. Besides nickel, other promoter metals such as

https://doi.org/10.1021/acssuschemeng.4c03279
ACS Sustainable Chem. Eng. 2024, 12, 9541−9549

Table 1. Integral Catalytic Performance (6.0 cm) of Pure and Metal-Promoted In_2O_3/ZrO_2 Catalysts at p = 50 bar (H_2/CO_2 = 3:1), T = 250 °C, and GHSV = 63.000 h^{-1},[a]

catalyst	S_{MeOH}/%	$P_{MeOH,active,metal}/g_{MeOH}\ g_{metal}^{-1}\ h^{-1}$	$P_{CO,active,metal}/g_{CO}\ g_{metal}^{-1}\ h^{-1}$	nominal H_2 reduction capacity	nominal CO_2 adsorption capacity
In_2O_3/ZrO_2	82 ± 0	1.60 ± 0.03	0.32 ± 0.00	1.00	1.00
$Ce-In_2O_3/ZrO_2$	89 ± 1	1.52 ± 0.02	0.17 ± 0.03	1.28	1.26
$Cu-In_2O_3/ZrO_2$	85 ± 2	1.90 ± 0.03	0.29 ± 0.05	1.52	0.70
Ni- In_2O_3/ZrO_2	80 ± 0	2.96 ± 0.04	0.63 ± 0.02	1.40	1.56

[a]Nominal H_2 Reduction and CO_2 Adsorption Capacity.

Table 2. Effect of Reaction Conditions on the Integral Catalytic Performance of $Ni-In_2O_3/ZrO_2$ at the Outlet (6.0 cm) of the Compact Profile Reactor Using a Feed Gas Composition of CO_2/H_2 = 1/3

parameter[a]	S_{MeOH}/%	$P_{MeOH,active,In+Ni}/g_{MeOH}\ g_{In+Ni}^{-1}\ h^{-1}$	$P_{CO,active,metal}/g_{CO}\ g_{In+Ni}^{-1}\ h^{-1}$
50 bar	80 ± 0	2.96 ± 0.04	0.63 ± 0.02
62.5 bar	81 ± 0	3.06 ± 0.03	0.61 ± 0.01
75 bar	81 ± 0	3.54 ± 0.07	0.70 ± 0.03
32,000 h^{-1}	79 ± 0	2.18 ± 0.01	0.52 ± 0.01
63,000 h^{-1}	80 ± 0	2.96 ± 0.04	0.63 ± 0.02
95,000 h^{-1}	84 ± 0	3.98 ± 0.03	0.67 ± 0.00
225 °C	83 ± 0	1.88 ± 0.02	0.33 ± 0.00
250 °C	80 ± 0	2.96 ± 0.04	0.63 ± 0.02
275 °C	73 ± 1	4.90 ± 0.01	1.57 ± 0.06

[a]Influence of total pressure at 250 °C and 63,000 h^{-1}, GHSV at 250 °C and 50 bar, and temperature at 50 bar and 63,000 h^{-1}.

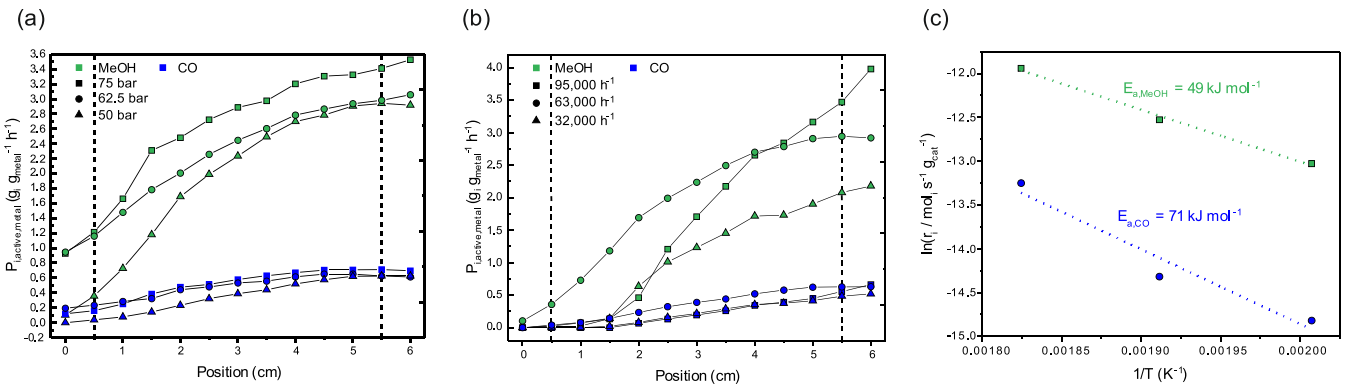

Figure 6. Influence of the reaction conditions on spatially resolved temperature and product profiles of $Ni-In_2O_3/ZrO_2$ using a feed gas composition of CO_2/H_2 = 1/3. The measurements were taken between 5 and 35 h TOS. (a) Pressure variation at T = 250 °C and GHSV = 63,000 h^{-1}. (b) GHSV variation at T = 250 °C and p = 50 bar and (c) apparent activation energies of MeOH (green) and CO (blue).

copper and cerium have been tested as well (Table 2). However, they showed a similar behavior in the CPR but were inferior in terms of methanol productivity compared to nickel doping, which underlines the outstanding performance of Ni as a promoter and correlates with the findings of H_2 TPR and CO_2 TPD. Moreover, all indium-based catalysts showed a significantly higher methanol selectivity (S = 80−90%) compared to the commercial CZA catalyst (S = 40%) under the applied reaction conditions. A summary of the integral catalytic performance (6.0 cm) for the metal-promoted and pure In_2O_3/ZrO_2 is shown in Table 1. More details on the spatial reaction profiles for copper- and cerium-promoted catalysts can be found in the Supporting Information (Figure S5).

Influence of Reaction Conditions on the Catalytic Performance of the $Ni-In_2O_3/ZrO_2$ Catalyst in the CPR. *Impact of Total Pressure.* The impact of total pressure on the catalytic performance in the CPR is generally in accordance with the principle of Le Chatelier. With an increase in pressure, the overall productivity of methanol is higher throughout the CPR (see Table 2 and Figure 6a). At 50 bar reaction pressure, the methanol productivity rises until a maximum productivity (2.92 $g_{MeOH}\cdot g_{In+Ni}^{-1}\cdot h^{-1}$) is achieved at the reactor outlet (6.0 cm). At 62.5 bar, an increase in methanol productivity (3.06 $g_{MeOH}\cdot g_{In+Ni}^{-1}\cdot h^{-1}$) past the catalyst bed could be observed. This could be increased to 3.53 $g_{MeOH}\cdot g_{In+Ni}^{-1}\cdot h^{-1}$ at 75 bar, indicating more headroom for the methanol generation due to the higher thermodynamic equilibrium conversion at higher pressure.[42] The steep slope of methanol production from the beginning of the catalyst bed to about 4 cm could be attributed to the parallel hydrogenation of CO_2 and CO coming from the parallel rWGS reaction. The gradient of methanol production between 4 and 5.5 cm decreases, as CO formation no longer increases. Methanol selectivity remains constant at approximately 80%, regardless of pressure. The rWGS is not affected by pressure according Le Chatelier's principle assuming an ideal gas. We observed a negligible impact of pressure for the CO production at the end of the catalyst bed. It is remarkable that the CO productivity reaches its highest point before the end of the catalyst bed (4.5 cm) and remains constant and

https://doi.org/10.1021/acssuschemeng.4c03279
ACS Sustainable Chem. Eng. 2024, 12, 9541−9549

even decreases at the end of the catalyst bed. Therefore, a higher overall pressure with a longer reaction bed could be favorable for both an increase in methanol selectivity and productivity.

Effect of Contact Time/Influence of the Gas Hourly Space Velocity (GHSV). Similar to the effect of increasing pressure, a higher methanol productivity can be observed for higher GHSVs, shorter residence time, and a reduction of the thickness of the diffusion boundary layer (Figure 6b). This means that a shorter contact time is favorable for methanol generation using the Ni−In_2O_3/ZrO_2 catalyst. This agrees with the results of In_2O_3/ZrO_2 that were shown in the previous literature. Higher GHSVs shift the selectivity toward methanol, while low contact times increase the MeOH production rate, keeping the CO formation constant.[16] According to the calculated Carberry number Ca = 0.03 (50 bar, 250 °C), the estimated extraparticle mass transfer does not limit the reaction rate (Ca < 0.05) at the boundary layer (detailed calculations are reported in the SI, Table S1 and eqs S6−S15).

As the GHSV increases, productivity seems to rapidly increase throughout the reaction profile. At 32,000 h^{-1}, the methanol productivity reaches 2.18 $g_{MeOH}{\cdot}g_{In+Ni}^{-1}{\cdot}h^{-1}$, increasing to 2.96 $g_{MeOH}{\cdot}g_{In+Ni}^{-1}{\cdot}h^{-1}$ at 63,000 h^{-1} until the end of the catalyst bed. A further increase of the GHSV to 95,000 h^{-1} resulted in a boost of methanol productivity up to 3.98 $g_{MeOH}{\cdot}g_{In+Ni}^{-1}{\cdot}h^{-1}$. The use of the CPR setup reveals a decrease in the temperature at the reactor inlet as the GHSV increases. The increase in heat dissipation is compensated by a higher reaction rate due to lower contact times, in turn leading to more reaction heat and an increase in the overall methanol productivity. If the gas feed is too high, cooling the catalyst bed below a threshold temperature of 238 °C, the reaction heat is not enough to keep the methanol reaction rate high, and the catalyst is almost completely inactive at first. If a temperature of 238 °C is reached, the catalyst is suddenly activated, showing a linear trend in methanol productivity to the end of the reactor (see Figure S6). With a better temperature control by preheating of the feed gas, the catalyst performance can be tweaked to reach even higher methanol productivities, while the commercial CZA catalyst has already reached the highest productivities at half the catalyst bed, producing more CO and reducing the methanol selectivity.

Effect of Temperature to Determine Apparent Activation Energies. Higher temperatures significantly favor the production of CO due to the endothermic rWGS reaction. At the reactor outlet (6.0 cm), an increase of CO productivity from 0.329 $g_{CO}{\cdot}g_{In+Ni}^{-1}{\cdot}h^{-1}$ at 225 °C to 1.58 $g_{CO}{\cdot}g_{In+Ni}^{-1}{\cdot}h^{-1}$ at 275 °C can be observed. This is in line with the selectivity of methanol, which decreases from 83% (225 °C) to 73% (275 °C). Due to higher reaction kinetics at higher temperature, the methanol productivity reaches its highest amount of 4.90 $g_{MeOH}{\cdot}g_{In+Ni}^{-1}{\cdot}h^{-1}$ in this study (see Table 2). The apparent activation energies ($E_{a,i}$) for methanol synthesis and the rWGS reaction (Figure 6c) were obtained from integral catalytic performance (6.0 cm) at different temperatures by using an Arrhenius plot. The methanol production requires less activation energy (49 kJ mol^{-1}) than CO production does (71 kJ mol^{-1}) using the Ni−In_2O_3/ZrO_2 catalyst in a CPR. This has also been revealed several times in the previous literature for fixed-bed reactors.[6,20,43] The activation energies show no limitations due to mass transport, as confirmed by the Ca number.

Post-mortem Characterization of the Ni-Promoted In_2O_3/ZrO_2 Catalysts. In order to round up this study, the properties of the best-performing Ni−In_2O_3/ZrO_2 catalyst after 90 h time on stream in the CPR were further investigated. The relative amount of indium (10.94%) and nickel (0.83%) determined by ICP-OES increased slightly, being in the range of its measurement accuracy. Therefore, no leaching due to the Mond process took place. The In_2O_3 particle size calculated using the (611) reflection patterns and the Scherrer equation (eq S5) was slightly reduced from 8.6 to 8.3 nm (see Figure S7) possibly due to surface attrition without sintering. The diffraction patterns before and after the reaction reveal no changes in morphology (see Figure S4). SEM-EDX mappings showed no agglomeration and well-dispersed indium and nickel distribution after the reaction (see Figure S8).

CONCLUSIONS

In this study, a compact profile reactor (CPR) was applied for the first time to study the differential reaction profiles along the reactor length for different methanol synthesis catalysts. Recording of the local temperature throughout the whole catalyst bed was also implemented at steady-state conditions. Reaction profiles of the state-of-the-art CZA catalyst showed a distinct hot spot of the catalyst bed at 2.5 cm, while the indium-based catalysts showed a more uniform temperature profile along the catalytic bed. This leads to better temperature control and reduces the risk of hot spots for In-based catalysts. The addition of nickel to In_2O_3/ZrO_2 increased the productivity of methanol from 1.60 $g_{MeOH}\ g_{Metal}^{-1}\ h^{-1}$ up to 2.96 $g_{MeOH}\ g_{Metal}^{-1}\ h^{-1}$ due to higher CO_2 adsorption capacity as well as promoted reducibility of the surface. The effect of different reaction conditions on the catalytic performance of Ni−In_2O_3/ZrO_2 using the CPR showed that higher pressure, GHSV, and temperature increased the methanol productivity. Since the Ni−In_2O_3/ZrO_2 catalyst is more selective and hinders the rWGS reaction, shorter contact times can therefore be beneficial for higher methanol yields. Contrarily, higher temperatures decrease methanol selectivity and shift the methanol yield to lower values. The CZA produced 3.46 $g_{MeOH}\ g_{Cu}^{-1}\ h^{-1}$ methanol but was overall less selective (58%) and prone to long-term deactivation. In addition, the Ni−In_2O_3/ZrO_2 catalysts exhibit a lower metal loading on the catalyst support compared to CZA. Our findings show that Ni−In_2O_3/ZrO_2 catalysts are highly promising for selective hydrogenation of CO_2 to methanol (80%) in a CPR.

ASSOCIATED CONTENT

Supporting Information

The Supporting Information is available free of charge at https://pubs.acs.org/doi/10.1021/acssuschemeng.4c03279.

Process flow diagram, supporting calculations, mass transfer limitation criteria, synthesis and characterization of metal-promoted In_2O_3/ZrO_2 catalysts, XRD patterns and SEM-EDX mappings, (611) reflection patterns of In_2O_3/ZrO_2-based catalysts, integration of H_2 TPR and CO_2 TPD curves, results and temperature gradient of other Ce- and Cu-promoted In_2O_3/ZrO_2 catalysts, supporting temperature profile at different GHSVs for the Ni-In_2O_3/ZrO_2 catalyst, and supporting postmortem characterization of the Ni-doped catalyst (PDF)

https://doi.org/10.1021/acssuschemeng.4c03279
ACS Sustainable Chem. Eng. 2024, 12, 9541−9549

AUTHOR INFORMATION

Corresponding Author

Jakob Albert − *Institute of Technical and Macromolecular Chemistry, Universität Hamburg, 20146 Hamburg, Germany;* orcid.org/0000-0002-3923-2269; Email: jakob.albert@uni-hamburg.de

Authors

Philipp Kampe − *Institute of Technical and Macromolecular Chemistry, Universität Hamburg, 20146 Hamburg, Germany;* orcid.org/0000-0001-8843-1240

Nick Herrmann − *Institute of Technical and Macromolecular Chemistry, Universität Hamburg, 20146 Hamburg, Germany;* orcid.org/0009-0003-8227-8654

Charlotte Ruhmlieb − *Institute of Physical Chemistry, Universität Hamburg, 20146 Hamburg, Germany*

Maik Finsel − *Reacnostics GmbH, 20457 Hamburg, Germany*

Oliver Korup − *Institute for Chemical Reaction Engineering, Hamburg University of Technology, 21073 Hamburg, Germany*

Raimund Horn − *Reacnostics GmbH, 20457 Hamburg, Germany; Institute for Chemical Reaction Engineering, Hamburg University of Technology, 21073 Hamburg, Germany*

Complete contact information is available at: https://pubs.acs.org/10.1021/acssuschemeng.4c03279

Author Contributions

⊥P.K. and N.H. contributed equally to this work and therefore share the first authorship.

Notes

The authors declare no competing financial interest.

ACKNOWLEDGMENTS

This project was funded by the Deutsche Forschungsgemeinschaft (DFG, German Research Foundation), SFB 1615-503850735. The authors thank the central analytics department and the X-ray Service Facility at Hamburg University for ICP-OES measurements and powder diffractograms. A special thanks to the department of electron microscopy for SEM-EDX measurements. We thank Dr. Michael Pabel from Saint-Gobain NorPro for the supply of ZrO_2. Open access funding was enabled and organized by Projekt DEAL.

REFERENCES

(1) Arrhenius, S. On the Influence of Carbonic Acid in the Air upon the Temperature of the Ground. *Philosophical Magazine J. Sci.* **1896**, *5*, 237−276.

(2) Schühle, P.; Schmidt, M.; Schill, L.; Riisager, A.; Wasserscheid, P.; Albert, J. Influence of gas impurities on the hydrogenation of CO_2 to methanol using indium-based catalysts. *Catal. Sci. Technol.* **2020**, *10*, 7309−7322.

(3) Cui, X.; Kær, S. K. A comparative study on three reactor types for methanol synthesis from syngas and CO_2. *Chem. Eng. J.* **2020**, *393*, No. 124632.

(4) Bozzano, G.; Manenti, F. Efficient methanol synthesis: Perspectives, technologies and optimization strategies. *Prog. Energy Combust. Sci.* **2016**, *56*, 71−105.

(5) Twigg, M. V.; Spencer, M. S. Deactivation of supported copper metal catalysts for hydrogenation reactions. *Appl. Catal., A* **2001**, *212*, 161−174.

(6) Klier, K.; Chatikavanij, V.; Herman, R. G.; Simmons, G. W. Catalytic Synthesis of Methanol from CO/H_2: The Effects of Carbon Dioxide. *J. Catal.* **1981**, *1982*, 343−360.

(7) *Chemical Technology*; Andreas Jess, P. W., Ed.; Wiley-VCH: Weinheim, 2013.

(8) Fichtl, M. B.; Schlereth, D.; Jacobsen, N.; Kasatkin, I.; Schumann, J.; Behrens, M.; Schlögl, R.; Hinrichsen, O. Kinetics of deactivation on $Cu/ZnO/Al_2O_3$ methanol synthesis catalysts. *Appl. Catal., A* **2015**, *502*, 262−270.

(9) Cui, X.; Kær, S. K. Thermodynamic Analyses of a Moderate-Temperature Process of Carbon Dioxide Hydrogenation to Methanol via Reverse Water−Gas Shift with In Situ Water Removal. *Ind. Eng. Chem. Res.* **2019**, *58*, 10559−10569.

(10) Schühle, P.; Reichenberger, S.; Marzun, G.; Albert, J. Slurry Phase Hydrogenation of CO_2 to Methanol Using Supported In_2O_3 Catalysts as Promising Approach for Chemical Energy Storage. *Chem. Ing. Tech.* **2021**, *93*, 585−593.

(11) Kampe, P.; Herrmann, N.; Wesner, A.; Ruhmlieb, C.; Albert, J. Catalyst and Parameter Optimization Study for Slurry-Phase Methanol Synthesis Using Ni-Doped Indium-Based Catalysts. *ACS Sustainable Chem. Eng.* **2023**, *11*, 14633−14644.

(12) Jiang, Y.; Yang, H.; Gao, P.; Li, X.; Zhang, J.; Liu, H.; Wang, H.; Wei, W.; Sun, Y. Slurry methanol synthesis from CO_2 hydrogenation over micro-spherical SiO_2 support Cu/ZnO catalysts. *J. CO2 Util.* **2018**, *26*, 642−651.

(13) Gaikwad, R.; Reymond, H.; Phongprueksathat, N.; Rudolf von Rohr, P.; Urakawa, A. From CO or CO_2?: space-resolved insights into high-pressure CO_2 hydrogenation to methanol over $Cu/ZnO/Al_2O_3$. *Catal. Sci. Technol.* **2020**, *10*, 2763−2768.

(14) Frei, M. S.; Mondelli, C.; Cesarini, A.; Krumeich, F.; Hauert, R.; Stewart, J. A.; Curulla Ferré, D.; Pérez-Ramírez, J. Role of Zirconia in Indium Oxide-Catalyzed CO_2 Hydrogenation to Methanol. *ACS Catal.* **2020**, *10*, 1133−1145.

(15) Gao, P.; Zhang, L.; Li, S.; Zhou, Z.; Sun, Y. Novel Heterogeneous Catalysts for CO_2 Hydrogenation to Liquid Fuels. *ACS Cent. Sci.* **2020**, *6*, 1657−1670.

(16) Martin, O.; Martín, A. J.; Mondelli, C.; Mitchell, S.; Segawa, T. F.; Hauert, R.; Drouilly, C.; Curulla-Ferré, D.; Pérez-Ramírez, J. Indium Oxide as a Superior Catalyst for Methanol Synthesis by CO_2 Hydrogenation. *Angew. Chem., Int. Ed.* **2016**, *55*, 6261−6265.

(17) Wesner, A.; Kampe, P.; Herrmann, N.; Eller, S.; Ruhmlieb, C.; Albert, J. Indium-based Catalysts for CO_2 Hydrogenation to Methanol: Key Aspects for Catalytic Performance. *ChemCatChem* **2023**, *15*, e202301125 DOI: 10.1002/cctc.202301125.

(18) Wang, J.; Zhang, G.; Zhu, J.; Zhang, X.; Ding, F.; Zhang, A.; Guo, X.; Song, C. CO_2 Hydrogenation to Methanol over In_2O_3-Based Catalysts: From Mechanism to Catalyst Development. *ACS Catal.* **2021**, *11*, 1406−1423.

(19) Jia, X.; Sun, K.; Wang, J.; Shen, C.; Liu, C. Selective hydrogenation of CO_2 to methanol over Ni/In_2O_3 catalyst. *J. Energy Chem.* **2020**, *50*, 409−415.

(20) Frei, M. S.; Mondelli, C.; García-Muelas, R.; Morales-Vidal, J.; Philipp, M.; Safonova, O. V.; López, N.; Stewart, J. A.; Ferré, D. C.; Pérez-Ramírez, J. Nanostructure of nickel-promoted indium oxide catalysts drives selectivity in CO_2 hydrogenation. *Nat. Commun.* **2021**, *12*, No. 1960.

(21) Zhang, Z.; Shen, C.; Sun, K.; Liu, C. Improvement in the activity of Ni/In_2O_3 with the addition of ZrO_2 for CO_2 hydrogenation to methanol. *Catal. Commun.* **2022**, *162*, No. 106386.

(22) Frei, M. S.; Mondelli, C.; García-Muelas, R.; Kley, K. S.; Puértolas, B.; López, N.; Safonova, O. V.; Stewart, J. A.; Curulla Ferré, D.; Pérez-Ramírez, J. Atomic-scale engineering of indium oxide promotion by palladium for methanol production via CO_2 hydrogenation. *Nat. Commun.* **2019**, *10*, No. 3377.

(23) Wei, Y.; Liu, F.; Ma, J.; Yang, C.; Wang, X.; Cao, J. Catalytic roles of In_2O_3 in ZrO_2-based binary oxides for CO_2 hydrogenation to methanol. *Molcular Catal.* **2022**, *525*, No. 112354.

(24) Tsoukalou, A. *Development of In_2O_3-Based Catalysts for the Hydrogenation of CO_2 to Methanol: Elucidating the Structure-Performance Relationship, Active Sites and Reaction Mechanism*; ETH Zurich, 2022.

(25) Sharma, P.; Hoang Ho, P.; Shao, J.; Creaser, D.; Olsson, L. Role of ZrO_2 and CeO_2 support on the In_2O_3 catalyst activity for CO_2 hydrogenation. *Fuel* **2023**, *331*, No. 125878.
(26) Cannizzaro, F.; Hensen, E. J. M.; Filot, I. A. W. The Promoting Role of Ni on In_2O_3 for CO_2 Hydrogenation to Methanol. *ACS Catal.* **2023**, *13*, 1875−1892.
(27) Tsoukalou, A.; Serykh, A. I.; Willinger, E.; Kierzkowska, A.; Abdala, P. M.; Fedorov, A.; Müller, C. R. Hydrogen dissociation sites on indium-based ZrO_2-supported catalysts for hydrogenation of CO_2 to methanol. *Catal. Today* **2022**, *387*, 38−46.
(28) Kampe, P.; Wesner, A.; Schühle, P.; Hess, F.; Albert, J. Effect of Conversion, Temperature and Feed Ratio on In_2O_3 /$In(OH)_3$ Phase Transitions in Methanol Synthesis Catalysts: A Combined Experimental and Computational Study. *ChemPlusChem* **2023**, *88*, No. e202300425.
(29) Lau, K.; Schühle, P.; Liang, S.-X.; Kock, F. de.; Albert, J.; Reichenberger, S. Laser-Generated InO_x/ZrO_2 Catalysts for CO_2 Hydrogenation: Role of In Situ Fragmentation and Ripening Control. *ACS Appl. Energy Mater.* **2021**, *4*, 9206−9215.
(30) Aquino, A.; Korup, O.; Horn, R. Liquid Phase Epoxidation of Propylene to Propylene Oxide with Hydrogen Peroxide on Titanium Silicalite-1: Spatially Resolved Measurements and Numerical Simulations. *Ind. Eng. Chem. Res.* **2023**, *62*, 3098−3115.
(31) Espinoza, D.; Wollak, B.; Sheppard, T. L.; Dippel, A.-C.; Sturm, M.; Gutowski, O.; Schmidt, M.; Korup, O.; Horn, R. Catalytic Profile Reactor for Multimodal Operando Measurements during Periodic Operation. *ChemCatChem.* **2022**, *14*, e202200337 DOI: 10.1002/cctc.202200337.
(32) Pottbacker, J.; Jakobtorweihen, S.; Behnecke, A. S.; Abdullah, A.; Özdemir, M.; Warner, M.; Menon, M.; Bujalski, J. M.; Waller, D.; Korup, O.; Horn, R. Resolving gradients in an ammonia oxidation reactor under industrial conditions: A combined experimental and simulation study. *Chem. Eng. J.* **2022**, *439*, No. 135350.
(33) Wollak, B.; Doronkin, D. E.; Espinoza, D.; Sheppard, T.; Korup, O.; Schmidt, M.; Alizadefanaloo, S.; Rosowski, F.; Schroer, C.; Grunwaldt, J.-D.; Horn, R. Exploring catalyst dynamics in a fixed bed reactor by correlative operando spatially-resolved structure-activity profiling. *J. Catal.* **2022**, *408*, 372−387.
(34) Monshi, A.; Foroughi, M. R.; Monshi, M. R. Modified Scherrer Equation to Estimate More Accurately Nano-Crystallite Size Using XRD. *WJNSE* **2012**, *02*, 154−160.
(35) Portillo, A.; Parra, O.; Aguayo, A. T.; Ereña, J.; Bilbao, J.; Ateka, A. Kinetic Model for the Direct Conversion of CO_2/CO into Light Olefins over an In_2O_3-ZrO2/SAPO-34 Tandem Catalyst. *ACS Sustainable Chem. Eng.* **2024**, *12*, 1616−1624.
(36) Nielsen, N. D.; Jensen, A. D.; Christensen, J. M. The roles of CO and CO_2 in high pressure methanol synthesis over Cu-based catalysts. *J. Catal.* **2021**, *393*, 324−334.
(37) Studt, F.; Behrens, M.; Kunkes, E. L.; Thomas, N.; Zander, S.; Tarasov, A.; Schumann, J.; Frei, E.; Varley, J. B.; Abild-Pedersen, F.; et al. The Mechanism of CO and CO_2 Hydrogenation to Methanol over Cu-Based Catalysts. *ChemCatChem* **2015**, *7*, 1105−1111.
(38) Wu, J.; Saito, M.; Takeuchi, M.; Watanabe, T. The stability of Cu/ZnO-based catalysts in methanol synthesis from a CO_2-rich feed and from a CO-rich feed. *Appl. Catal., A* **2001**, *218*, 235−240.
(39) Tsoukalou, A.; Bushkov, N. S.; Docherty, S. R.; Mance, D.; Serykh, A. I.; Abdala, P. M.; C., Copéret; A., Fedorov; C. R., Müller. *Surface Intermediates in In-Based ZrO_2-Supported Catalysts for Hydrogenation of CO_2 to Methanol.*.
(40) Ye, J.; Liu, C.; Mei, D.; Ge, Q. Active Oxygen Vacancy Site for Methanol Synthesis from CO_2 Hydrogenation on In_2O_3 (110): A DFT Study. *ACS Catal.* **2013**, *3*, 1296−1306.
(41) Shen, H.; Li, H.; Yang, Z.; Li, C. Magic of hydrogen spillover: Understanding and application. *Green Energy & Environment* **2022**, *7*, 1161−1198.
(42) Stangeland, K.; Li, H.; Yu, Z. Thermodynamic Analysis of Chemical and Phase Equilibria in CO_2 Hydrogenation to Methanol, Dimethyl Ether, and Higher Alcohols. *Ind. Eng. Chem. Res.* **2018**, *57*, 4081−4094.
(43) Araújo; Mondelli; Pinheiro; Thaylan, C.; Agrachev, M.; Zou, T.; Willi, P. O.; Engel, K. M.; Grass, R. N.; Stark, W. J.; Safonova, O. V.; Jeschke, G.; et al. Flame-made ternary Pd-In_2O_3-ZrO_2 catalyst with enhanced oxygen vacancy generation for CO_2 hydrogenation to methanol. *Nat. Commun.* **2022**, *13*, No. 5610, DOI: 10.1038/s41467-022-33391-w.

https://doi.org/10.1021/acssuschemeng.4c03279
ACS Sustainable Chem. Eng. 2024, 12, 9541−9549